



OPEN ACCESS

EDITED BY

Paolo Remondelli,
University of Salerno, Italy

REVIEWED BY

Francesca Zappa,
Altos labs, United States
Erik Alexander Blackwood,
University of Arizona, United States

*CORRESPONDENCE

Fabiola Osorio,
✉ fabiolaosorio@med.uchile.cl

[†]These authors have contributed equally to this work and share first authorship

SPECIALTY SECTION

This article was submitted to Signaling, a section of the journal Frontiers in Cell and Developmental Biology

RECEIVED 04 November 2022

ACCEPTED 08 March 2023

PUBLISHED 21 March 2023

CITATION

Gutiérrez-Ballesteros F, Morales-Reyes J, Fernández D, Geisse A, Arcaya A, Flores-Santibañez F, Bono MR and Osorio F (2023), Normal tissue homeostasis and impairment of selective inflammatory responses in dendritic cells deficient for ATF6 α . *Front. Cell Dev. Biol.* 11:1089728. doi: 10.3389/fcell.2023.1089728

COPYRIGHT

© 2023 Gutiérrez-Ballesteros, Morales-Reyes, Fernández, Geisse, Arcaya, Flores-Santibañez, Bono and Osorio. This is an open-access article distributed under the terms of the [Creative Commons Attribution License \(CC BY\)](https://creativecommons.org/licenses/by/4.0/). The use, distribution or reproduction in other forums is permitted, provided the original author(s) and the copyright owner(s) are credited and that the original publication in this journal is cited, in accordance with accepted academic practice. No use, distribution or reproduction is permitted which does not comply with these terms.

Normal tissue homeostasis and impairment of selective inflammatory responses in dendritic cells deficient for ATF6 α

Francisca Gutiérrez-Ballesteros^{1†}, Jonathan Morales-Reyes^{1†}, Dominique Fernández¹, Antonia Geisse¹, Amada Arcaya¹, Felipe Flores-Santibañez¹, María Rosa Bono² and Fabiola Osorio^{1*}

¹Laboratory of Immunology and Cellular Stress, Immunology Program, Institute of Biomedical Sciences, Faculty of Medicine, University of Chile, Santiago, Chile, ²Immunology Laboratory, Biology Department, Faculty of Sciences, University of Chile, Santiago, Chile

The initiation of adaptive immunity relies on the performance of dendritic cells (DCs), which are specialized leukocytes with professional antigen presenting capabilities. As such, the molecular mechanisms safeguarding DC homeostasis are matter of intense research. Sensors of the unfolded protein response (UPR) of the endoplasmic reticulum, a three-pronged signaling pathway that maintains the fidelity of the cellular proteome, have emerged as regulators of DC biology. The archetypical example is the IRE1/XBP1s axis, which supports DC development and survival of the conventional type 1 DC (cDC1) subtype. However, the role of additional UPR sensors in DC biology, such as the ATF6 α branch, has not been clearly elucidated. Even though *Xbp1* is transcriptionally induced by ATF6 α under ER stress, it is unclear if cDCs also co-opt the ATF6 α branch in tissues. Here, we examine the role of ATF6 α in cDC homeostasis *in vivo* and upon innate stimulation *in vitro*. In steady state, animals lacking ATF6 α in CD11c⁺ cells (*Itgax* Cre x *Atf6*^{fl/fl} mice) display normal cDC frequencies in spleen, intestine, liver, and lung. Also, ATF6 α deficient cDCs express normal levels of *Xbp1* mRNA and additional UPR components. However, a reduction of lung monocytes is observed in *Itgax* Cre x *Atf6*^{fl/fl} conditional deficient animals suggesting that ATF6 α may play a role in the biology of monocyte subsets. Notably, in settings of DC activation, ATF6 α contributes to the production of IL-12 and IL-6 to inflammatory stimuli. Thus, although ATF6 α may be dispensable for tissue cDC homeostasis in steady state, the transcription factor plays a role in the acquisition of selective immunogenic features by activated DCs.

KEYWORDS

dendritic cells, unfolded protein response, ATF6, tissues, immunity, proinflammatory cytokines, IL-12, IL-6

Introduction

Dendritic cells (DCs) are chief sentinels of the immune system responsible to couple innate and adaptive immunity (Cabeza-Cabrerizo et al., 2021). DCs are a heterogeneous family of leukocytes that include plasmacytoid DCs (pDCs, known to promote antiviral immunity), and conventional DCs (cDC), which are divided into type 1 cDCs (cDC1) and type 2 cDCs (cDC2) (Murphy et al., 2016). Due to their heightened capacity to activate CD8⁺

T cells against tumors and virally-infected cells, cDC1s have become central targets in immunotherapy whereas cDC2s are prone to activate CD4⁺ T cells against extracellular bacteria, fungi, and parasites (Murphy et al., 2016).

The capacity of DCs to orchestrate antigen specific immune responses has fostered scientific efforts to better understand molecular mechanisms safeguarding DC function. An emerging intracellular pathway regulating DC biology is the unfolded protein response (UPR), a response that maintains the fidelity of the cellular proteome in conditions eliciting endoplasmic reticulum (ER) stress, such as in infection, chronic inflammation and metabolic dysregulation (Grootjans et al., 2016; Smith et al., 2020). The UPR is initiated by three ER resident sensors: PERK (protein kinase R-like ER kinase), IRE1 (inositol-requiring enzyme 1, Alpha) and ATF6 (Activating transcription factor 6). PERK activation promotes attenuation of global protein translation, selective activation of amino acid metabolism/oxidative stress genes and the coordination of cell death via the pro-apoptotic transcription factor CHOP (Grootjans et al., 2016; Hetz et al., 2020). IRE1 is an enzyme bearing a serine-threonine kinase and endoribonuclease (RNase) domain, which mediates unconventional splicing of *Xbp1u* mRNA (X box binding protein 1, unspliced), prompting the translation of XBP1s (XBP1 spliced), a potent transcription factor and key activator of ER biogenesis, lipid biosynthesis and chaperone genes (Grootjans et al., 2016; Read and Schröder, 2021). In addition, in poorly defined conditions of ER stress, IRE1 RNase can degrade diverse mRNAs/microRNAs through a mechanism known as “regulated IRE1-dependent decay” (RIDD) (Hetz et al., 2020).

ATF6 is a member of the bZIP family with two homologous proteins, ATF6 α (encoded by the *Atf6* gene) and ATF6 β in mammals (Haze et al., 1999; Yoshida et al., 2001; Adachi et al., 2008; Almanza et al., 2019). ATF6 α is a potent transcription factor known to control expression of genes coding for chaperones, lipid biosynthesis and ERAD (ER Associated Degradation) members in contexts of ER stress (Thuerlauf et al., 2002; Yamamoto et al., 2004; Sharma et al., 2019). In contrast, the role of ATF6 β is less understood, and it is proposed to possess weaker transcriptional activity than ATF6 α (Yoshida et al., 1998; Yoshida et al., 2000; Thuerlauf et al., 2004; Thuerlauf et al., 2007). ATF6 β has also shown to counteract ATF6 α transcriptional activity (Thuerlauf et al., 2004) and to date, ATF6 α is the predominant isoform controlling cellular responses during ER stress settings (Glembotski et al., 2019).

Interestingly, the UPR branches can be also co-regulated to safeguard protein homeostasis (Shoulders et al., 2013). For instance, ATF6 α controls expression of *Xbp1* (Yoshida et al., 2000; Yoshida et al., 2001), and ATF6 α and XBP1s can also form heterodimers that regulate expression of selected proteostatic genes (Yamamoto et al., 2007; Shoulders et al., 2013; Vidal et al., 2021). Notably, despite this knowledge, the interplay between ATF6 α and XBP1s has not been extended *in vivo* to tissue resident cells.

Regarding DC subtypes, pDCs and cDCs are highly sensitive to perturbations in UPR components and require IRE1/XBP1s signaling for development (Iwakoshi et al., 2007; Flores-Santibáñez et al., 2019). In differentiated stages, cDC1s display constitutive IRE1 RNase activity (Osorio et al., 2014) and selectively depend on IRE1/XBP1s signaling for survival in tissues such as the lung (Tavernier et al., 2017). PERK also controls certain DC/cDC1 functions, which is evidenced by high rate of eIF2 α

phosphorylation in steady state cDC1s (Mendes et al., 2020). Furthermore, in contexts of DC activation, the IRE1/XBP1s and PERK branches are critical to fine tune immunogenic features of activated DCs (Mogilenko et al., 2019). As such, DCs selectively activate UPR components but to date, there is no evidence addressing the role of ATF6 α in DC biology. This is a relevant question considering that DC subtypes are increasingly studied in their capacity to fine tune UPR components to regulate immunity. Here, we studied cDC homeostasis in tissues from animals bearing selective deletion of ATF6 α in DCs. Our data shows that mice lacking ATF6 α in DCs display normal cDC composition in lymphoid and non-lymphoid organs. We also observe that ATF6 α deficient cDCs expressed normal levels of *Xbp1s* and additional UPR components. However, ATF6 α deficiency in CD11c⁺ cells resulted in reduced frequencies of lung monocytes, suggesting that the transcription factor may influence the biology of monocyte subtypes in tissues. Finally, in contexts of DC activation with inflammatory stimuli, our data reveal a contribution of ATF6 α in the production of IL-12 and IL-6 by bone marrow-derived DCs. Altogether, our data indicate that the UPR sensor ATF6 α does not control influence tissue DC homeostasis in steady state, but it selectively tunes the production of specific proinflammatory cytokines in contexts of activation.

Results

ATF6 α deficiency does not alter cDC composition in the spleen

To obtain insights on the role of ATF6 α in DC homeostasis, we generated conditional *knock-out* animals lacking ATF6 α in CD11c-expressing cells. To this end, we crossed the *Itgax*-Cre mice line with *Atf6*^{fl/fl} mice (referred to as “ATF6 α ^{ADC} mice”) (Engin et al., 2013). These animals delete exons 8-9 of *Atf6* in CD11c-expressing cells (which fully targets cDC1s and cDC2s, while partially targeting pDCs and monocyte/macrophage subsets (Abram et al., 2014)). ATF6 α ^{ADC} mice are compared to control animals (*Atf6*^{fl/fl} littermates with no expression of Cre, scheme depicted in Figure 1A). Spleen cDCs were isolated from ATF6 α ^{ADC} mice and control animals and expression of ATF6 α was quantified by qPCR (Figure 1B). As expected, cDC1s and cDC2s from ATF6 α ^{ADC} mice do not express *Atf6* mRNA and maintain normal expression of *Atf6b*, validating the model of study. Next, we analyzed the composition of cDC1s and cDC2s and observed that ATF6 α ^{ADC} mice display unaltered frequencies of these subtypes (Figures 1C, D). Furthermore, cellular composition analysis of ATF6 α ^{ADC} mice in spleen revealed that these animals have normal composition of immune cell types (Figure 1E, gating analysis in Supplementary Figure S1).

To assess whether ATF6 α deficient cDCs undergo normal differentiation/activation, we quantified expression of the costimulatory molecules PD-L1, CD86 and CD40, which are surface immunoregulatory molecules that allow cDCs to restrain or activate T cells, respectively (Kapsenberg, 2003; Hubo et al., 2013). Data in Figure 1F show that ATF6 α deficiency does not alter surface expression of these proteins in cDCs. In conclusion, ATF6 α does not regulate the differentiation/activation program of steady state cDCs in spleen.

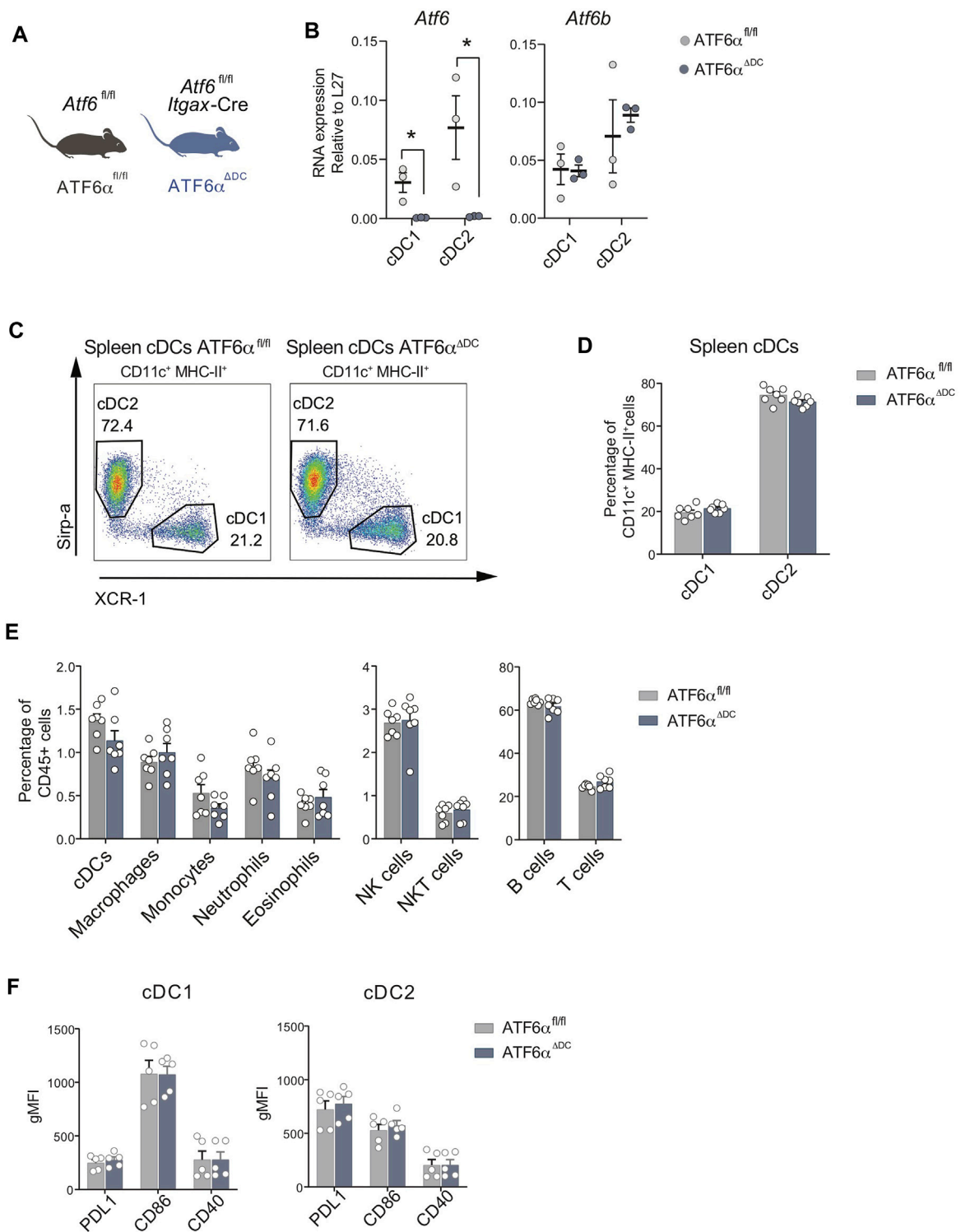
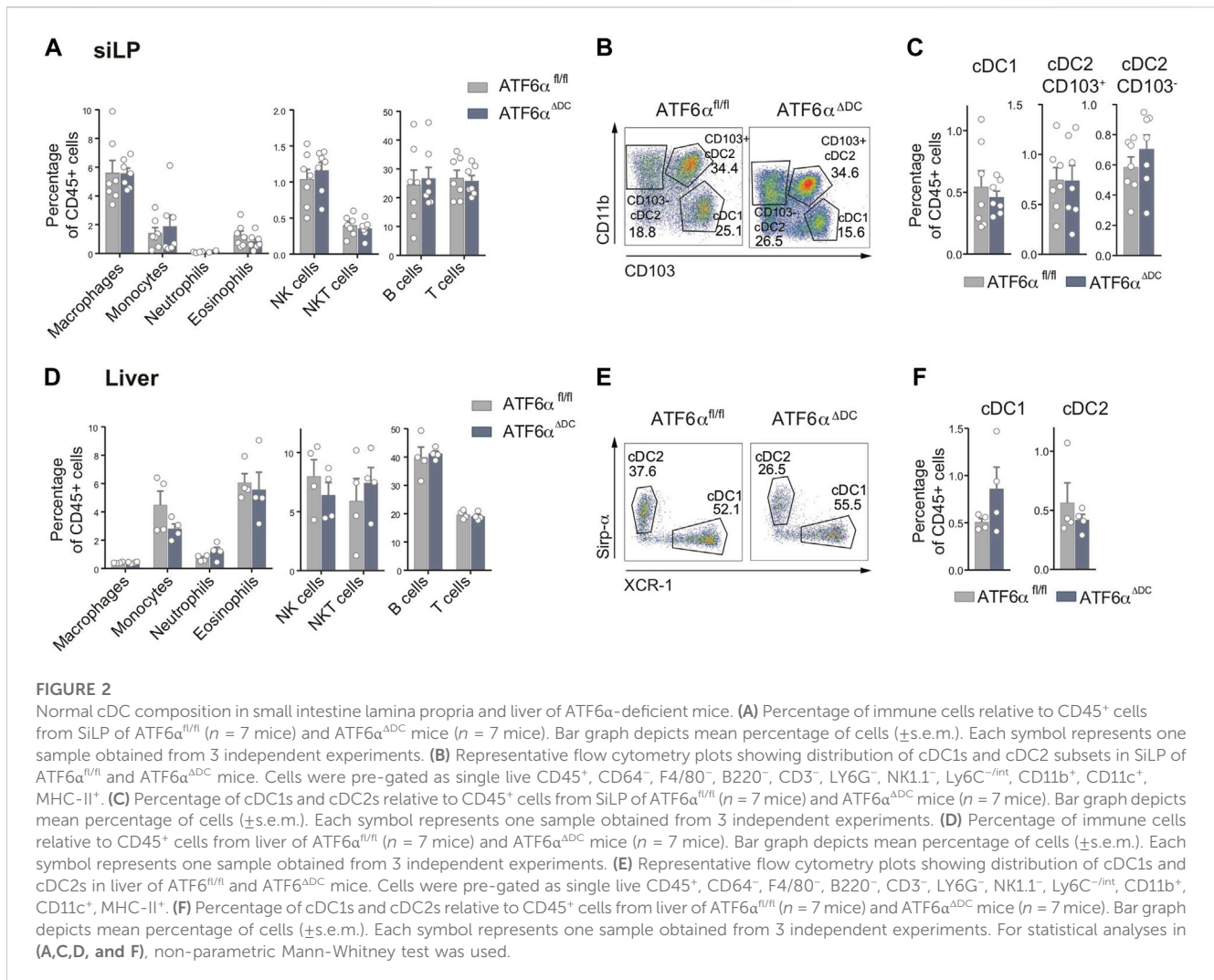


FIGURE 1

ATF6 α deficiency does not alter cDC composition in spleen. **(A)** Schematic representation of ATF6 α ^{ADC} mouse model. **(B)** Quantification of L27-relative expression of *Atf6* and *Atf6b* mRNA in cDC1s and cDC2s sorted from spleen of ATF6 α ^{fl/fl} ($n = 3$ mice) and ATF6 α ^{ADC} mice ($n = 3$ mice). Quantification was performed by qPCR. Each symbol represents one mouse obtained from two independent experiments. **(C)** Representative flow cytometry plots showing distribution of cDC1s and cDC2s in spleen of ATF6 α ^{fl/fl} and ATF6 α ^{ADC} mice. Cells were pre-gated as single live CD45⁺, CD64⁺, F4/80⁺, B220⁺, CD3⁺, LY6G⁺, NK1.1⁺, Ly6C^{int}, CD11b⁺, CD11c⁺, MHC-II⁺. **(D)** Percentage of cDC1s and cDC2s relative to CD11c⁺ MHC-II⁺ cells in spleen of ATF6 α ^{fl/fl} ($n = 7$ mice) and ATF6 α ^{ADC} mice ($n = 7$ mice). Each symbol represents one sample obtained from 3 independent experiments. **(E)** Percentage of cDCs, macrophages, monocytes, neutrophils, eosinophils, NK, NKT, B and T cells relative to the total percentage of CD45⁺ cells in spleen of ATF6 α ^{fl/fl} ($n = 7$ mice) and ATF6 α ^{ADC} mice ($n = 7$ mice). Bar graph depicts mean percentage of cells (\pm s.e.m.). Each symbol represents one sample obtained from 3 independent experiments. **(F)** Quantification of costimulatory molecules in cDC1s and cDC2s from spleen of ATF6 α ^{fl/fl} ($n = 5$ mice) and ATF6 α ^{ADC} mice ($n = 5$ mice). The identification of co-stimulatory molecules was carried out by labeling with antibodies. Each symbol represents the sample obtained from a mouse in three independent experiments. For statistical analyses in **(B–F)** a non-parametric Mann-Whitney test was used, $*p < 0.05$.



Normal DC composition in the small intestine lamina propria and liver of ATF6 α ^{ADC} mice

Considering that cDCs in lymphoid organs are not equivalent to counterparts exposed to inflammatory stimuli in non-lymphoid tissues, we analyzed cDCs from the small intestine lamina propria (SiLP) and liver of ATF6 α ^{ADC} mice (Figure 2, gating analysis Supplementary Figures S1A, B). We verified that archetypical immune cell types were present in normal frequencies in the SiLP of ATF6 α ^{ADC} mice (Figure 2A). In the SiLP, *bona-fide* cDCs are divided in cDC1s (defined as CD103⁺CD11b⁻) and two subsets of cDC2s (CD103⁺CD11b⁺ and CD103⁻CD11b⁺) (Sun et al., 2020). Analysis of ATF6 α ^{ADC} mice show normal frequencies of the three cDC subtypes at the SiLP (Figures 2B–C). Liver tissue analysis show similar results, normal immune cell composition (Figure 2D, gating analysis in Supplementary Figure S2B) and comparable cDC frequencies between ATF6 α deficient and control counterparts (Figures 2E, F). Altogether, these data indicate that ATF6 α loss does not impair cDC homeostasis in tissues.

Deletion of ATF6 α does not recapitulate XBP1 deficiency in lung cDCs

The *Xbp1* gene is a transcriptional ATF6 α target that contains an ER stress response element (ERSE) consensus sequence on its promoter region (Yoshida et al., 2000). Phenotypically, XBP1 deficiency in DCs leads to a marked reduction in cDC1 frequencies in the lung (Tavernier et al., 2017). The interplay between ATF6 α and XBP1s led us to hypothesize that ATF6 α ^{ADC} mice may recapitulate the loss of lung cDC1s observed in XBP1 conditional deficient mice. To test this hypothesis, we generated conditional knock-out animals lacking XBP1s in CD11c-expressing cells by crossing the *Itgax*-Cre mice line with *Xbp1*^{fl/fl} mice (Lee et al., 2008) (referred to as “XBP1^{ADC} mice”). Lung cDCs from XBP1^{ADC} mice, ATF6 α ^{ADC} mice and control littermates were analyzed by flow cytometry (Figures 3A–D). We observed that ATF6 α ^{ADC} mice display comparable lung cDC1 percentages with control counterparts (Figures 3A, B). However, these observations were not recapitulated in XBP1^{ADC} mice, which revealed an evident loss of cDC1s compared to control littermates, confirming previous findings (Tavernier et al., 2017) (Figures 3C, D). These data indicate

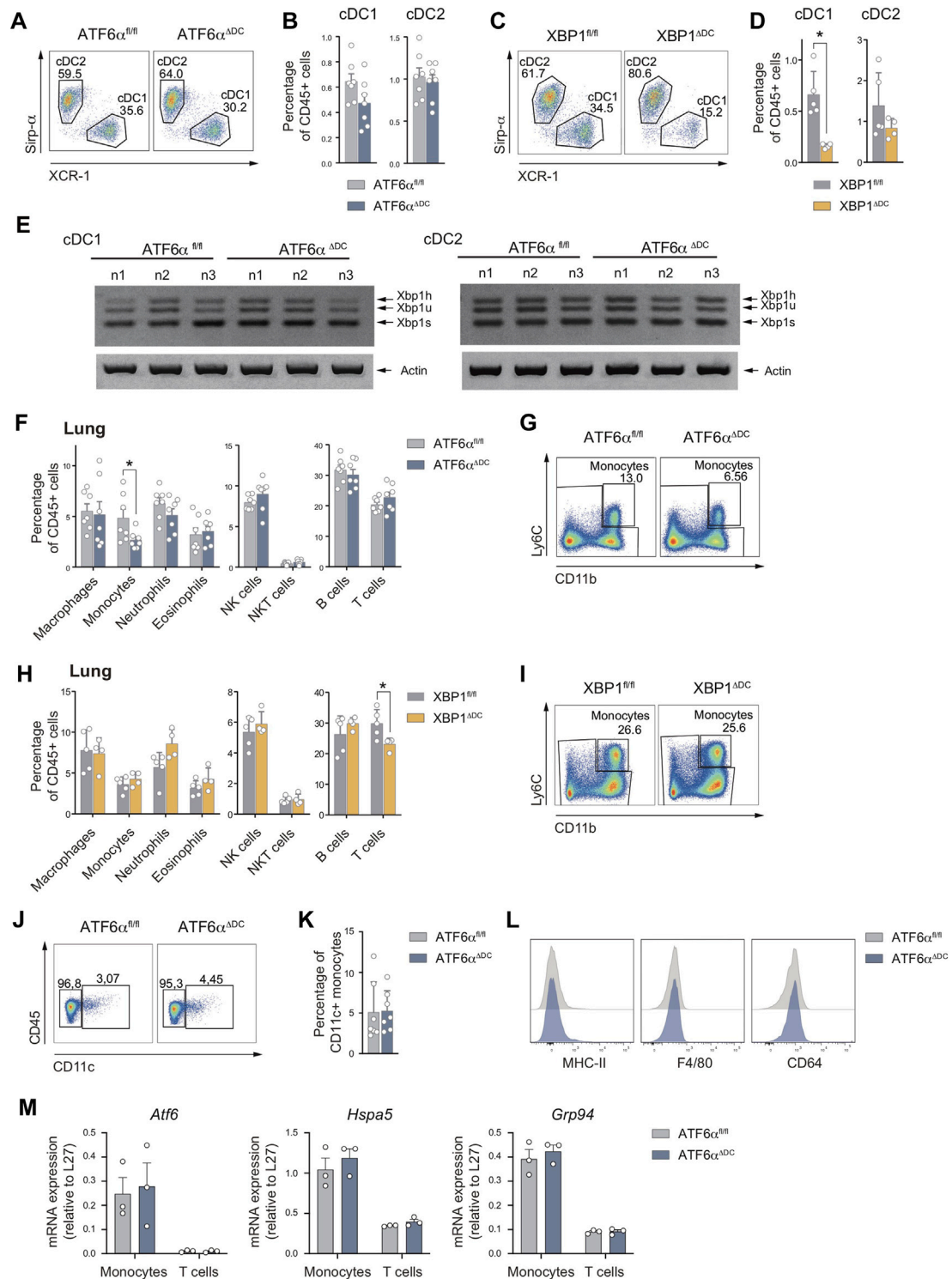


FIGURE 3

The loss of lung cDC1s observed upon XBP1 deletion is not recapitulated by deficiency of ATF6α (A) Representative flow cytometry plots showing distribution of cDC1s and cDC2s in lung of *ATF6α^{fl/fl}* and *ATF6α^{ΔDC}* mice. (B) Percentage of cDC1s and DC2s relative to CD45⁺ cells from lung of *ATF6α^{fl/fl}* (n = 7 mice) and *ATF6α^{ΔDC}* mice (n = 7 mice). Bar graph depicts mean percentage of cells (±s.e.m.). Each symbol represents one sample obtained from 3 independent experiments. (C) Representative flow cytometry plots showing distribution of cDC1s and cDC2s in lung of *XBP1^{fl/fl}* and *XBP1^{ΔDC}* mice. (D) Percentage of cDC1s and DC2s relative to CD45⁺ cells from lung of *XBP1^{fl/fl}* (n = 5 mice) and *XBP1^{ΔDC}* mice (n = 4 mice). Bar graph depicts mean percentage of cells (±s.e.m.). Each symbol represents one sample obtained from two independent experiments. (E) RT-PCR analysis of *Xbp1* splicing in cDC1s and cDC2s sorted from spleen of *ATF6α^{fl/fl}* (n = 3 mice) and *ATF6α^{ΔDC}* mice (n = 3 mice). Data were obtained from two independent experiments. *Xbp1h*: *Xbp1* hybrid, *Xbp1u*: *Xbp1* unspliced, *Xbp1s*: *Xbp1* spliced. Actin (bottom) serves as a loading control. (F) Percentage of immune cells relative to CD45⁺ cells from lung of *ATF6α^{fl/fl}* (n = 7 mice) and *ATF6α^{ΔDC}* mice (n = 7 mice). Bar graph depicts mean percentage of cells (±s.e.m.). Each symbol represents one sample obtained from 3 independent experiments. (G) Representative flow cytometry plots showing monocytes from lung of *ATF6α^{fl/fl}* (Continued)

FIGURE 3 (Continued)

and ATF6 α^{ADC} mice. (H) Percentage of immune cells relative to CD45 $^{+}$ cells from lung of XBP1 $^{\text{fl/fl}}$ ($n = 5$ mice) and XBP1 $^{\text{ADC}}$ mice ($n = 4$ mice). Bar graph depicts mean percentage of cells (\pm s.e.m.). Each symbol represents one sample obtained from two independent experiment. (I) Representative flow cytometry plots showing lung monocytes from XBP1 $^{\text{fl/fl}}$ and XBP1 $^{\text{ADC}}$ mice. (J) Representative flow cytometry plots showing CD11c expression by lung monocytes from ATF6 $\alpha^{\text{fl/fl}}$ and ATF6 α^{ADC} mice. (K) Percentage of CD11c $^{+}$ lung monocytes from ATF6 $\alpha^{\text{fl/fl}}$ ($n = 7$ mice) and ATF6 α^{ADC} mice ($n = 7$ mice). Bar graph depicts mean percentage of cells (\pm s.e.m.). Each symbol represents one sample obtained from 3 independent experiments. (L) Representative flow cytometry plots showing MHC-II, F4/80 and CD64 expression by lung monocytes from ATF6 $\alpha^{\text{fl/fl}}$ and ATF6 α^{ADC} mice. (M) Quantification of *Atf6*, *Hspa5* and *Grp94* expression in monocytes and T cells sorted from lung of ATF6 $\alpha^{\text{fl/fl}}$ ($n = 3$ mice) and ATF6 α^{ADC} mice ($n = 3$ mice) by qPCR. Each symbol represents one mouse. For statistical analyses in (B,D,F,H,K, and M), non-parametric Mann-Whitney test was used.

that despite reported evidence demonstrating transcriptional regulation of *Xbp1* by ATF6 α (Yoshida et al., 2001), the *in vivo* functional outcomes of these transcription factors in tissue DCs do not overlap. To explain these results, we investigated if ATF6 α deficient DCs express altered levels of *Xbp1* mRNA. PCR analysis of sorted splenic cDC subsets revealed that ATF6 α -deficient cDC1s and cDC2s express normal levels of *Xbp1u* and *Xbp1s* (Figure 3E), indicating that ATF6 α deficiency does not alter XBP1 expression in tissue cDCs.

We also quantified the composition of additional lung immune cells in ATF6 α^{ADC} mice. Interestingly, analysis revealed a significant reduction in the frequencies of lung monocytes compared to control mice (Figures 3F, G). Notably, this reduction was not observed in XBP1 $^{\text{ADC}}$ mice (Figures 3H, I), suggesting that ATF6 α and XBP1s regulate the fate of myeloid cells by independent mechanisms. These findings prompted us to investigate whether wild-type lung monocytes show signs of ATF6 α transcriptional activity in steady state. To this end, we quantified expression of *Atf6* mRNA and the ATF6 α targets *Hspa5* (BiP) and *Grp94* by qPCR in isolated lung monocytes from control animals, and transcript levels were compared with those measured in lung T cells (Figure 3M, grey bars). Data indicated that lung monocytes tend to express higher levels of *Atf6*, *Hspa5* and *Grp94* than T cells isolated from the same tissue, suggesting that the former cell type show signs of ATF6 α transcriptional activity in the steady state lung.

Finally, to evaluate if the remaining population of lung monocytes from ATF6 α^{ADC} mice display signs of cellular dysregulation, we measured expression of canonical surface molecules and ATF6 α targets by flow cytometry and qPCR, respectively. These cells express normal levels CD11c, MHC-II, CD64 and F4/80 (Figure 3J–L), and were CD11c $^{\text{int}}$ MHC-II $^{\text{lo/+}}$ CD64 $^{\text{lo}}$ F4/80 $^{\text{lo}}$, in line with the definition of Ly6C $^{+}$ pulmonary monocytes (Gibbins et al., 2017). In addition, lung monocytes from ATF6 α^{ADC} mice expressed similar levels of *Atf6*, *Hspa5* and *Grp94* than control animals, suggesting that the remanent monocyte population from ATF6 α^{ADC} mice are not targeted by Cre-mediated recombination (Figure 3M). To sum up, these data suggest that lung monocytes show signs of basal ATF6 α transcriptional activity and that ATF6 α loss in CD11c $^{+}$ cells result in partial reduction of lung monocyte frequencies.

ATF6 α deficiency in steady state cDCs does not alter expression of UPR components

Finally, given that ATF6 α does not control expression of *Xbp1u/s* in cDCs (Figure 3E), we sought to investigate whether ATF6 α could regulate expression of additional UPR components in these cells. To this end, target genes of the ATF6 α , PERK and IRE1 (XBP1s and RIDD

targets) branches were quantified by qPCR in cDC1s and cDC2s isolated from spleen of ATF6 α^{ADC} and ATF6 α^{WT} mice (Figure 4). Data show that ATF6 α deficient cDC1s express a trend towards reduced *Hspa5* expression, which did not reach statistical significance (Figure 4A). Furthermore, ATF6 α deficient cDCs express unaltered levels of the XBP1s targets *Erdj4* and *Edem1* (Figure 4B), the RIDD substrates *Cd18* and *Bloc1s1* (Figure 4C) and the PERK targets *Chop*, *Atf4* and *Gadd34* (Figure 4D). Notably, cDCs from ATF6 α^{ADC} mice also expressed normal levels of the reported ATF6 targets *HerpUD* and *Grp94* (Figure 4E). These data show that cDCs do not constitutively activate the ATF6 α branch in steady state. Furthermore, these observations indicate that in absence of canonical ER stress, ATF6 α does not regulate expression of UPR components in cDCs *in vivo*.

ATF6 α regulate the production of the proinflammatory cytokines IL-12 and IL-6 during DC activation

Finally, we sought to evaluate if ATF6 α regulates the acquisition of immunogenic features in contexts of DC activation. To this end, we studied bone-marrow derived DCs cultured in presence of the differentiation factor GM-CSF (referred to as ‘GM-DCs’). We corroborate that GM-DC cultures of ATF6 α^{ADC} mice generate normal proportion of DCs (Figure 5A) and display *Atf6* ablation without interfering with *Atf6b* expression (Figure 5B). To determine ATF6 α transcriptional activity, we treated GM-DCs from ATF6 α^{ADC} and control mice with the pharmacological ER stressor tunicamycin (Figure 5C). As expected, tunicamycin treatment induces activation of the ATF6 α targets *HerpUD* and *Grp94*, and expression of these transcripts are reduced in GM-DCs deficient for ATF6 α (Figure 5C), validating the model of study. Next, we interrogated if ATF6 α contributes to the acquisition of immunogenic features during DC activation. For this purpose, we studied two types of stimuli; R848 (Resiquimod, an imidazoquinoline agonist of toll-like receptor 7 -TLR7 that possesses antiviral activity), and R848 combined with palmitic acid (R848/PA), which is a saturated fatty acid reported to induce activation of XBP1s, ATF4 and CHOP in activated DCs, potentiating their immunogenic function (Mogilenko et al., 2019). Our data indicate that both R848 and R848/PA elicit competent GM-DC activation by means of CD86 expression (Figure 5D). However, only R848/PA induces persistent BiP induction in GM-DCs (Figure 5E), confirming that the mixed stimuli trigger sustained UPR activation in these cells. As reported (Mogilenko et al., 2019), R848/PA also induced efficient activation of XBP1s y PERK branches (Supplementary Figure 4A), so we sought to investigate if R848/PA was also competent to trigger ATF6 α transcriptional activity. Data depicted in Figure 5F shows that R848/PA efficiently

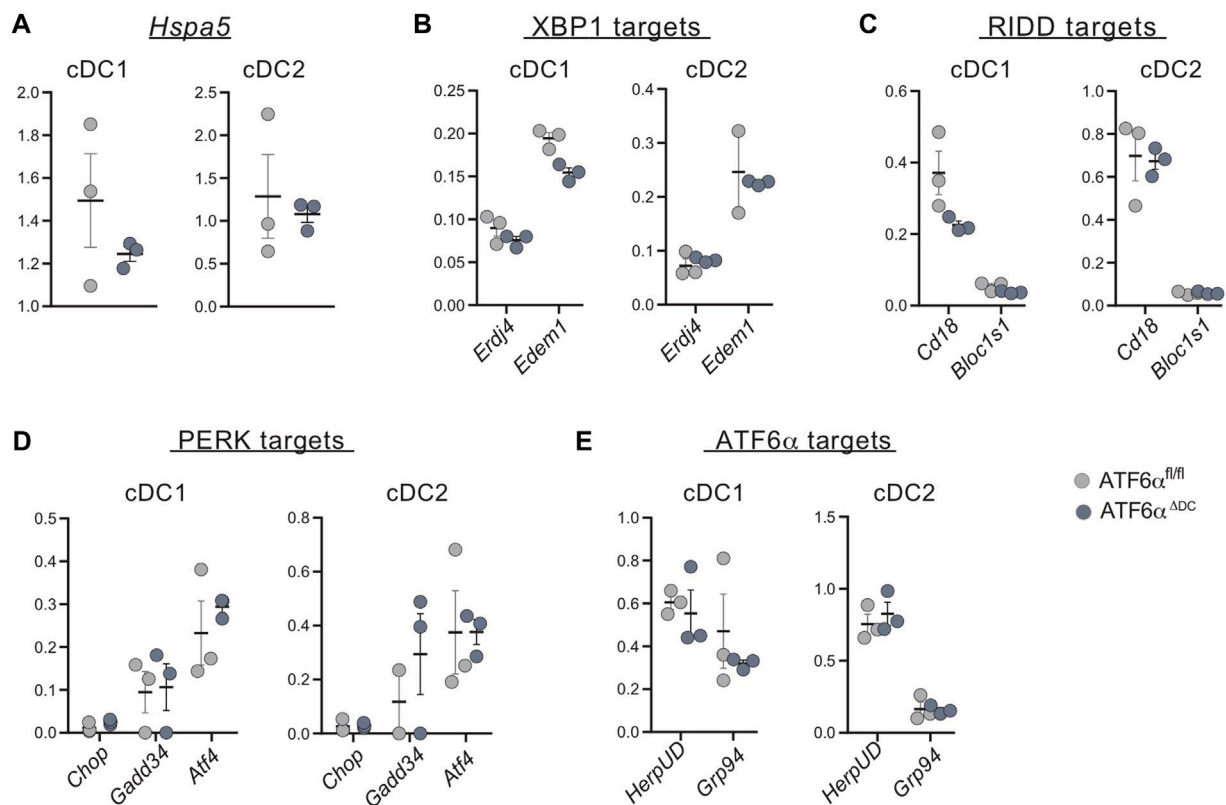


FIGURE 4

ATF6 α deficient cDCs express normal level of UPR components. qPCR analysis of basal expression of UPR target genes from sorted spleen cDCs of ATF6 $\alpha^{fl/fl}$ ($n = 3$ mice) and ATF6 $\alpha^{\Delta DC}$ mice ($n = 3$ mice). (A) Expression of *Hspa5* (BiP) was used as a readout of ER stress, and specific target genes of (B) IRE1-XBP1 axis, (C) RIDD branch, (D) PERK and (E) ATF6 α pathways were quantified by qPCR. RNA expression was normalized to housekeeping genes L27. Each symbol represents the sample obtained from one mouse in two independent experiments. For statistical analyses, the non-parametric Mann-Whitney test was used.

induce *HerpUD* and *Grp94* expression in GM-DCs in an ATF6 α dependent manner, confirming that the mixed stimuli activate the transcription factor in DCs. To connect these findings with a functional role, we investigated if ATF6 α regulates cytokine production in activated DCs. GM-DCs from ATF6 $\alpha^{\Delta DC}$ and control mice were stimulated with R848, R848/PA or vehicle and the production of proinflammatory cytokines was determined on mRNA and protein level. As reported (Mogilenko et al., 2019), PA treatment markedly augments the expression of *Il-23p19* mRNA in R848-stimulated GM-DCs, although we found that expression of the cytokine is not regulated by ATF6 α (Supplementary Figure 4B). IL-23 belongs to the IL-12 family of cytokines, in which IL-12 is a broadly studied factor involved in the generation of T helper 1 and natural killer responses, among others (Gee et al., 2009). The bioactive IL-12 form (termed IL-12p70) is comprised of the IL-12p35 and IL-12p40 subunits, in which the latter component is shared with IL-23 (IL-23p19/IL-12p40) (Gee et al., 2009). We observed that R848/PA stimulation also led to a significant increase in *Il-12p35* mRNA expression compared to R848 alone (Figure 5G). Interestingly, compared to control GM-DCs, ATF6 α deficient cells show decreased *Il-12p35* mRNA expression upon R848/PA stimulation (Figure 5G). To extend these findings to protein level, we quantified IL-12p70 secreted in the supernatants

of activated GM-DCs. Data depicted in Figure 5H shows that ATF6 α -deficient GM-DCs stimulated with R848/PA secrete lower levels of IL-12p70 compared to control counterparts. These data indicate that ATF6 α regulates IL-12 production by activated DCs. Next, we analyzed expression of additional proinflammatory cytokines and found that IL-6 was also reduced in the supernatants from ATF6 α knock-out GM-DCs stimulated with R848 or R848/PA (p -value = 0.06) (Figure 5I). Notably, we found no regulation of *Il-6* mRNA transcript levels by ATF6 α (Supplementary Figure 4C), suggesting regulation of the cytokine on translational/posttranslational level. Furthermore, the regulation of ATF6 α on cytokine production was not extended to all proinflammatory cytokines as TNF, another factor produced by activated GM-DCs was not regulated by the transcription factor (Figure 5J; Supplementary Figure 4D). Altogether, these findings demonstrate that ATF6 α selectively contributes to the production of IL-12p70 and IL-6 in DCs activated with inflammatory triggers.

Discussion

ATF6 α is a main UPR sensor known for coordinating ER stress responses, which is also emerging as a novel regulator in several

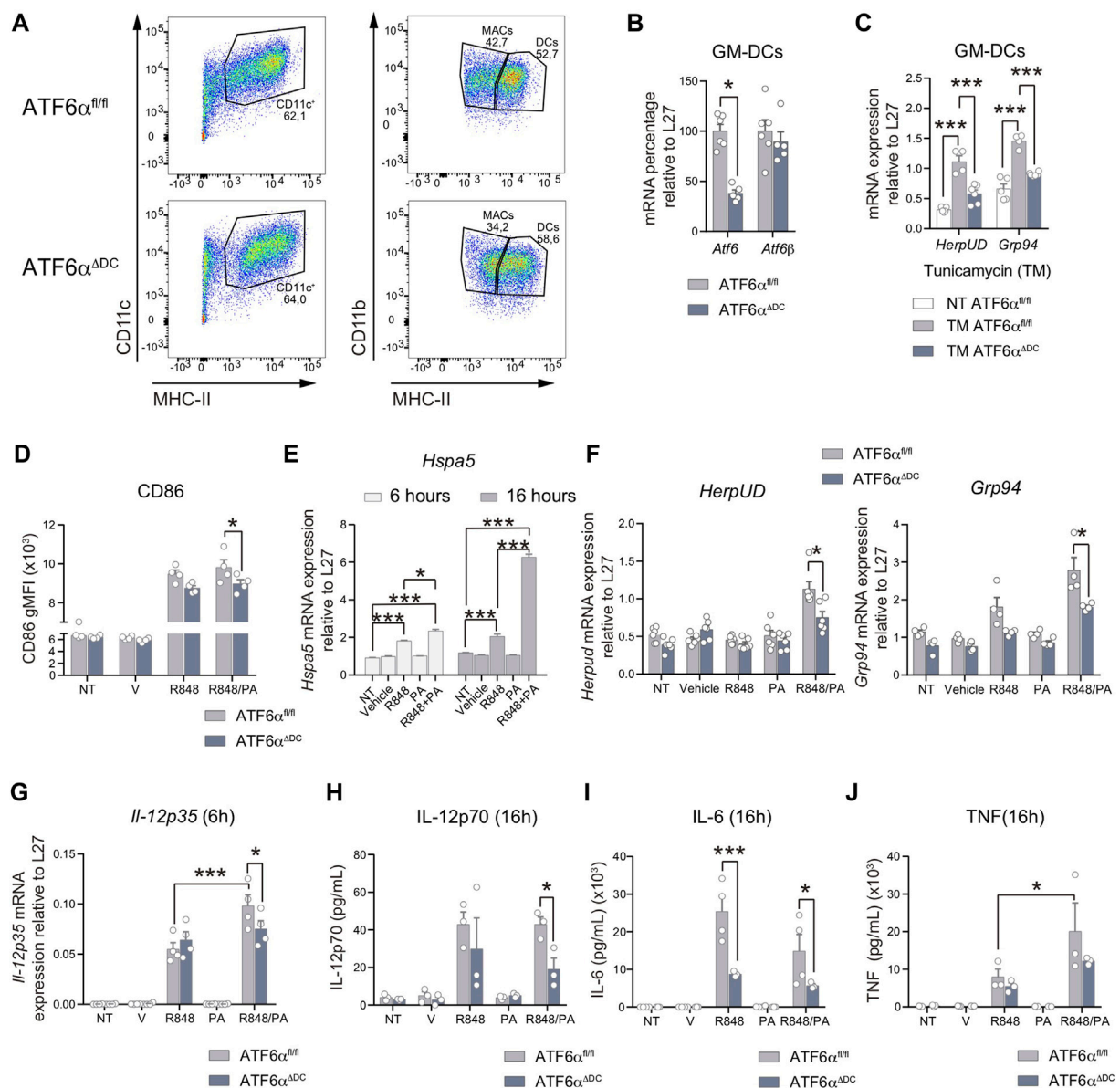


FIGURE 5

ATF6 α regulates IL-12 and IL-6 production by activated DCs (A) Representative flow cytometry plots of GM-DCs from ATF6 $\alpha^{fl/fl}$ and ATF6 α^{ADC} mice. Cells were gated as singlets, live, CD11b $^+$, CD11c $^+$, MHC-II $^+$. (B) Quantification of *Atf6* and *Atf6b* mRNA in GM-DCs from ATF6 $\alpha^{fl/fl}$ and ATF6 α^{ADC} mice ($n = 5-6$). (C) Expression of the ATF6 α targets *Herpud* and *Grp94* in ATF6 α sufficient or deficient GM-DCs stimulated with tunicamycin (TM) ($n = 3$). (D) Flow cytometry analysis of CD86 in GM-DCs from ATF6 $\alpha^{fl/fl}$ and ATF6 α^{ADC} mice stimulated with R848 (5 μ g/mL) with or without palmitic acid (0,5 mM, PA) for 16 h. GM-DCs were pre-gated as singlets, live, CD11b $^+$, CD11c $^+$, MHC-II high . (E) Expression of *Hspa5* (BiP) mRNA in GM-DCs from ATF6 $\alpha^{fl/fl}$ activated with the indicated stimuli for 6 and 16 h. (F) Expression of *Herpud* and *Grp94* in GM-DCs from ATF6 $\alpha^{fl/fl}$ and ATF6 α^{ADC} mice and activated with the indicated stimuli for 24 h ($n = 4-6$). (G) *Il-12p35* mRNA expression in GM-DCs from ATF6 $\alpha^{fl/fl}$ and ATF6 α^{ADC} mice and activated with the indicated stimuli for 6 h ($n = 4$). Measurement of secreted cytokines IL-12p70 (H), IL-6 (I), TNF (J) from supernatants of GM-DCs from ATF6 $\alpha^{fl/fl}$ and ATF6 α^{ADC} mice, and stimulated for 16 h ($n = 3, 4$). For statistical analyses, a non-parametric Mann-Whitney test was used, * $p < 0.05$.

pathologies (Hillary and Fitzgerald, 2018). ATF6 α roles have been implicated in adipogenesis, neural and muscular embryogenesis, retina development, foveal disease and heart failure, among others (Hillary and Fitzgerald, 2018; Blackwood et al., 2019; Correll et al., 2019; Lee et al., 2020; Kroeger et al., 2021). However, in cells of the immune system, the contribution of ATF6 α has not been extensively studied. Here, we studied the role of ATF6 α in DCs from tissues and from *in-vitro* cultures, which are known to activate UPR

components during development, function, and survival (Osorio et al., 2014; Tavernier et al., 2017; Mendes et al., 2020). Using conditional deficient mice for ATF6 α in the CD11c $^+$ compartment, we show that loss of the transcription factor does not alter cDC frequencies in lymphoid and non-lymphoid organs, and it does not regulate expression of activation markers in steady state. These findings differentiate ATF6 α from the additional UPR sensors IRE1 and PERK, which display specific cellular functions in

cDCs (Osorio et al., 2014; Tavernier et al., 2017; Mendes et al., 2020). Furthermore, data obtained with ATF6 α conditional deficient mice in DCs did not functionally emulate the loss of XBP1 in DCs, which severely impacts cDC1 survival in the lung (Tavernier et al., 2017). Indeed, ATF6 α deficient DCs from spleen express normal levels of *Xbp1u/s*, suggesting that additional mechanisms promote XBP1 expression in DCs. Whether these observations can be explained by functional compensation between ATF6 α and ATF6 β remains to be confirmed. Even though ATF6 α plays protective roles in pathological settings such as those induced by ischemia/reperfusion damage in several organs [(Blackwood et al., 2019), and reviewed in (18)], synergistic effects between ATF6 α and ATF6 β have also been reported in development (Yamamoto et al., 2007) and cardiac failure settings (Correll et al., 2019). In fact, ATF6 β has shown to play overlapping roles with ATF6 α in settings of heart hypertrophy (Correll et al., 2019). These data suggest that the interactions and functional outcomes of ATF6 α and ATF6 β *in vivo* may diverge to the observations made *in vitro* systems. Future work should elucidate whether tissue DC homeostasis is co-regulated by ATF6 α /ATF6 β interactions. In addition, our data show that ATF6 α deficiency did not alter expression of UPR components in DCs, even in targets of ATF6 α branch. This evidence indicates that in absence of ER stress, steady state cDCs do not spontaneously activate the ATF6 α transcriptional core of genes, differentiating this UPR module from the IRE1/XBP1s and PERK branches (Osorio et al., 2014; Tavernier et al., 2017; Mendes et al., 2020).

An aspect emerging from this work is that ATF6 α loss in CD11c⁺ expressing cells resulted in a decrease of monocyte frequencies in the lung. Lung monocytes are a heterogeneous population of cells and a subgroup of pulmonary monocytes are reported to express CD11c (Gibbins et al., 2017). Therefore, the decrease in monocyte frequencies in the lungs of ATF6 α ^{ADDC} mice could be due to direct effects in monocyte subtypes targeted by the *Itgax*-Cre mice line, as previous work shows that the mice line display an efficiency of 30% approx. Of Cre-mediated deletion in peripheral blood monocytes (Abram et al., 2014). The question as to why the reduction in monocyte frequencies in ATF6 α ^{ADDC} mice is selectively noticed in the lung compared to other tissues remains to be elucidated. Future studies using selective Cre-transgenic lines that allow optimal targeting of the monocyte population will help addressing the contribution of ATF6 α in monocyte biology.

Finally, we uncover a novel role for ATF6 α in settings of DC activation. Upon stimulation with a mix of TLR ligands and saturated fatty acids, cultured DCs become activated and induce the ATF6 α branch of the UPR, which contribute to the production of IL-12. These observations complement previous findings showing that IL-23, another member of the IL-12 family of cytokines, is optimally produced by DCs *via* a XBP1-ATF4-CHOP dependent mechanism (Mogilenko et al., 2019). Our findings identify IL-12 as an additional cytokine produced upon TLR ligand/fatty acid stimulation and identify ATF6 α as a regulator of the process. The molecular mechanisms accounting for IL-12 regulation by ATF6 α remain to be further investigated, as we did not find canonical ERSE and ERSE-II motifs in the promoter regions of the *Il12a* and *Il12b* genes (data not shown). Furthermore, we also observe that IL-6 production displays

ATF6 α dependency, even in conditions lacking saturated fatty acids. Importantly, the regulation of cytokine production by ATF6 α is not extended to all inflammatory factors, as TNF is not controlled by ATF6 α expression. On the other hand, the data presented here suggest that targeting ATF6 α may be beneficial in selective contexts of inflammation that evoke an IL-12/IL-6 cytokine response, which may include infection with intracellular bacteria or certain autoimmune contexts (Ge et al., 2009). Understanding the mechanisms underlying selective cytokine production by UPR components is critical to translate these findings to clinically relevant settings. From this work, it emerges the notion that there may be a “division of labor” among UPR sensors in the regulation of cytokine production to inflammatory settings.

Materials and methods

Experimental model and subject details

Mice

ATF6 α ^{WT} (ATF6fl/fl (Engin et al., 2013), obtained from The Jackson Laboratory), ATF6 α ^{ADDC} (ATF6fl/fl x *Itgax*-Cre (Caton et al., 2007)), XBP1^{WT} (XBP1fl/fl (Lee et al., 2008)), XBP1^{ADDC} (XBP1fl/fl x *Itgax*-Cre (Caton et al., 2007)), mice were bred at Universidad de Chile and Fundación Ciencia y Vida in specific pathogen-free conditions. All mice were kept on a C57BL/6 background. Litters with mice of both sexes at 10–14 weeks of age were used for experiments.

Method details

Preparation of cell suspensions

Spleens and livers were minced and digested in PBS supplemented with 10% FBS with Collagenase D (1 mg/mL, Roche) and DNase I (50 μ g/mL, Roche) for 30 min at 37°C in a water bath. Digested tissue was then passed through a 70 μ m cell strainer, followed by red blood cell lysis with RBC lysis buffer (Biolegend). Single cells were kept on ice.

Lungs were minced and digested in RPMI 1640 with Liberase TM (0.02 mg/mL; Roche) and DNase I (50 μ g/mL, Roche) for 30 min at 37°C in a water bath, resuspending the tissue with help of a Pasteur pipette every 10 min during the incubation. Digested tissue was then passed through a 70 μ m cell strainer, followed by red blood cell lysis with RBC lysis buffer (Biolegend). Single cells were kept on ice.

Intestines were cleaned with HBSS and the mesenteric lymph node, fat, and Peyer's patches were removed. Tissue was incubated for 20 min at 37°C with constant stirring at 100 rpm in RPMI 1640 medium supplemented with 1M DTT (Thermo Fisher Scientific), 0,5 M EDTA (Thermo Fisher Scientific). Tissues were minced and incubated in RPMI 1640 medium supplemented with liberase TL 12,5 mg/mL, (Roche), DNase I 10 mg/mL for 30 min at 37°C with constant stirring at 100 rpm and then smashed through a 40 mm sterile strainer. SiLP cells were centrifuged (700 g, 20 min, 25°C) in 2 step percoll (GE Healthcare) gradients (40% and 75%). Leukocytes were enriched in the 40%–75% edge fraction.

For cDCs sorting, spleens were minced and digested as previously described and the single-cell suspension was enriched prior to cell sorting by depletion of CD3e and B220 expressing cells using biotin-labeled monoclonal antibodies, anti-biotin microbeads and isolation kits (Miltenyi Biotec).

Flow cytometry and cell sorting

For surface staining, cells were incubated with anti-Fc receptor antibody and then stained with fluorochrome-conjugated antibodies in FACS buffer (PBS + 1% FBS + 2 mM EDTA) for 20 min at 4°C. Viability was assessed by staining with fixable viability Zombie UV (BioLegend). A biotinylated antibody was used for F4/80 staining, followed by a second staining step with Streptavidin-BUV737 (BD Biosciences) for 20 min at 4°C. Flow cytometry was performed on BD LSR Fortessa (BD Biosciences) instruments using FACSDiva software (BD Biosciences). Analysis of flow cytometry data was done using FlowJo software. Cell sorting was performed using FACS Aria III (BD Biosciences). Antibody clones used in this study are illustrated in [Supplementary Methods](#).

RNA isolation, cDNA generation and qPCR analysis

Total RNA was extracted from sorted spleen cDCs, lung monocytes and T cells with the RNeasy Micro Kit (Qiagen) following manufacturer's instructions. Total RNA from GM-DCs was extracted using TRizol reagent (Invitrogen). cDNA was prepared using M-MLV reverse transcriptase (Invitrogen). qPCR was performed with a SYBR Green PCR Master Mix kit (Applied Biosystems). (See [Supplementary Methods](#) for primers used for qPCR).

Xbp1s splicing assay

Total RNA was isolated by RNeasy plus Micro Kit (Qiagen) following manufacturer's instructions. cDNA was prepared using M-MLV reverse transcriptase (Invitrogen). The following primers were used for conventional PCR amplification of total *Xbp1* spliced and *Xbp1* unspliced: Fwd: 5'-ACACGCTTGGGAATGGACAC-3' and Rev: 5'-CCATGGGAAGATGTTCTGGG-3' (Martinon et al., 2010); and for beta actin (*Actb*): Fwd: 5'-CTAAGCCAACCGTGAAAAG-3' and Rev: 5'-TTGCTGATCCACATCTGCTG-3'. PCR products were analyzed on 2.8% agarose gels.

Bone marrow-derived DC cultures (GM-DCs)

3×10^6 bone marrow cells were seeded in 10 mL of complete medium (RPMI 1640 glutaMAX (Gibco), supplemented with penicillin/streptomycin (100 µg/mL, Corning), 2-mercaptoethanol (50 µM, Gibco), 10% heat-inactivated fetal bovine serum (Hyclone), and recombinant GM-CSF (20 ng/mL, Biolegend). Cells were incubated at 37°C in 5% CO₂. On day 3, 10 mL of complete medium containing GM-CSF (20 ng/mL) was added to the plate. On day 6, half of the medium was removed, and it was replaced by fresh medium supplemented with GM-CSF. Cells (GM-DCs) were harvested on day 9 and used for experiments.

Activation of GM-DCs

GM-DCs were activated with R848 (5 µg/mL, Invivogen) with or without palmitic acid (PA, 0.5 mM, Sigma) conjugated

with BSA (molar ratio PA:BSA 6:1, Sigma). Controls were RPMI (non-treated, NT), vehicle (BSA 0.083 mM with 0.5 mM ethanol). For cytometric bead array (CBA) assay (BD Biosciences), GM-DCs were cultured at 1×10^6 /mL in complete medium for 16 h. The supernatant was collected, and cytokines were quantified following manufacturer's instructions. For UPR activation with tunicamycin, GM-DCs were cultured as above, and cells were stimulated with tunicamycin (1 µg/mL, Sigma) for 8 h.

Quantification and statistical analysis

Statistical analysis was conducted using GraphPad Prism software (v9.1.2). Results are presented as mean \pm SEM. Two groups were compared using non-parametric two-tailed Mann-Whitney test as indicated in figure legends. A *p*-value < 0.05 was considered statistically significant.

Study approval

All animal procedures were approved and performed in accordance with institutional guidelines for animal care of the Fundación Ciencia y Vida and the Faculty of Medicine, University of Chile, and were approved by the local ethics committee.

Data availability statement

The raw data supporting the conclusion of this article will be made available by the authors, without undue reservation.

Ethics statement

All animal procedures were approved by the local ethics committee and performed in accordance with institutional guidelines for animal care of the Fundación Ciencia y Vida and the Faculty of Medicine, University of Chile.

Author contributions

FG-B, JM-R, and FO designed the research, FG-B, AG, AA, JM-R, FF, and DF did the experiments, FG-B, JM-R, DF, AG, AA, FF, MRB, and FO analysed and interpreted the results. MRB provided technical assistance and experimental expertise. FO wrote the manuscript.

Funding

This work was funded by an International Research Scholar Grant From HHMI (HHMI#55008744, FO); FONDECYT Grant No 1200793 (FO); FONDECYT Grant No 1191438 (MR.B); CONICYT/FONDEQUIP/EQM140016; ANID Grant FB210008 (MR.B).

Acknowledgments

We thank Dr Laurie H. Glimcher (Dana-Farber Cancer Institute) for *Xbp1^{fl/fl}* mice. We thank the facilities at Universidad de Chile and Fundación Ciencia & Vida. We thank members of the immunology and immunology and cellular stress laboratories for critical support.

Conflict of interest

The authors declare that the research was conducted in the absence of any commercial or financial relationships that could be construed as a potential conflict of interest.

References

- Abram, C. L., Roberge, G. L., Hu, Y., and Lowell, C. A. (2014). Comparative analysis of the efficiency and specificity of myeloid-Cre deleting strains using ROSA-EYFP reporter mice. *J. Immunol. Methods* 408, 89–100. doi:10.1016/j.jim.2014.05.009
- Adachi, Y., Yamamoto, K., Okada, T., Yoshida, H., Harada, A., and Mori, K. (2008). ATF6 is a transcription factor specializing in the regulation of quality control proteins in the endoplasmic reticulum. *Cell Struct. Funct.* 33 (1), 75–89. doi:10.1247/csf.07044
- Almanza, A., Carlesso, A., Chintha, C., Creedican, S., Doultinos, D., Leuzzi, B., et al. (2019). Endoplasmic reticulum stress signalling – from basic mechanisms to clinical applications. *FEBS J.* 286 (2), 241–278. doi:10.1111/febs.14608
- Blackwood, E. A., Azizi, K., Thuerauf, D. J., Paxman, R. J., Plate, L., Kelly, J. W., et al. (2019). Pharmacologic ATF6 activation confers global protection in widespread disease models by reprogramming cellular proteostasis. *Nat. Commun.* 10 (1), 187–216. doi:10.1038/s41467-018-08129-2
- Cabeza-Cabrero, M., Cardoso, A., Minutti, C. M., Pereira, M., and Reis e Sousa, C. (2021). Dendritic cells revisited. *Annu. Rev. Immunol.* 39 (1), 131–166. doi:10.1146/annurev-immunol-061020-053707
- Caton, M. L., Smith-Raska, M. R., and Reizis, B. (2007). Notch-RBP-J signaling controls the homeostasis of CD8⁺ dendritic cells in the spleen. *J. Exp. Med.* 204 (7), 1653–1664. doi:10.1084/jem.20062648
- Correll, R. N., Grimes, K. M., Prasad, V., Lynch, J. M., Khalil, H., and Molkentin, J. D. (2019). Overlapping and differential functions of ATF6α versus ATF6β in the mouse heart. *Sci. Rep.* 9 (1), 2059–2068. doi:10.1038/s41598-019-39515-5
- Engin, F., Yermalovich, A., Ngyuen, T., Hummasti, S., Fu, W., Eizzirik, D. L., et al. (2013). Restoration of the unfolded protein response in pancreatic β cells protects mice against type 1 diabetes. *Sci. Transl. Med.* 5 (211), 211ra156. doi:10.1126/scitranslmed.3006534
- Flores-Santibáñez, F., Medel, B., Bernales, J. I., and Osorio, F. (2019). Understanding the role of the unfolded protein response sensor IRE1 in the biology of antigen presenting cells. *Cells* 8 (12), 1563. doi:10.3390/cells8121563
- Gee, K., Guzzo, C., Mat, N. F. C., Ma, W., and Kumar, A. (2009). The IL-12 family of cytokines in infection, inflammation and autoimmune disorders. *Inflamm. Allergy - Drug Targets.* 8 (1), 40–52. doi:10.2174/187152809787582507
- Gibbins, S. L., Thomas, S. M., Atif, S. M., McCubbrey, A. L., Desch, A. N., Danhorn, T., et al. (2017). Three unique interstitial macrophages in the murine lung at steady state. *Am. J. Respir. Cell Mol. Biol.* 57 (1), 66–76. doi:10.1165/rcmb.2016-0361OC
- Glembotski, C. C., Rosarda, J. D., and Wiseman, R. L. (2019). Proteostasis and beyond: ATF6 in ischemic disease. *Trends Mol. Med.* 25 (6), 538–550. doi:10.1016/j.molmed.2019.03.005
- Grootjans, J., Kaser, A., Kaufman, R. J., and Blumberg, R. S. (2016). The unfolded protein response in immunity and inflammation. *Nat. Rev. Immunol.* 16 (8), 469–484. doi:10.1038/nri.2016.62
- Haze, K., Yoshida, H., Yanagi, H., Yura, T., and Mori, K. (1999). Mammalian transcription factor ATF6 is synthesized as a transmembrane protein and activated by proteolysis in response to endoplasmic reticulum stress. *Mol. Biol. Cell* 10 (11), 3787–3799. doi:10.1091/mbc.10.11.3787
- Hetz, C., Zhang, K., and Kaufman, R. J. (2020). Mechanisms, regulation and functions of the unfolded protein response. *Nat. Rev. Mol. Cell Biol.* 21, 421–438. doi:10.1038/s41580-020-0250-z
- Hillary, R. F., and Fitzgerald, U. (2018). A lifetime of stress: ATF6 in development and homeostasis. *J. Biomed. Sci.* 25 (1), 48–10. doi:10.1186/s12929-018-0453-1
- Hubo, M., Trinschek, B., Kryczanowsky, F., Tuettenberg, A., Steinbrink, K., and Jonuleit, H. (2013). Costimulatory molecules on immunogenic versus tolerogenic human dendritic cells. *Front. Immunol.* 4, 82–14. doi:10.3389/fimmu.2013.00082
- Iwakoshi, N. N., Pypaert, M., and Glimcher, L. H. (2007). The transcription factor XBP-1 is essential for the development and survival of dendritic cells. *J. Exp. Med.* 204 (10), 2267–2275. doi:10.1084/jem.20070525
- Kapsenberg, M. L. (2003). Dendritic-cell control of pathogen-driven T-cell polarization. *Nat. Rev. Immunol.* 3 (12), 984–993. doi:10.1038/nri1246
- Kroeger, H., Grandjean, J. M. D., Chiang, W. C. J., Bindels, D. D., Mastey, R., Okalova, J., et al. (2021). ATF6 is essential for human cone photoreceptor development. *Proc. Natl. Acad. Sci. U. S. A.* 118 (39), e2103196118–e2103196119. doi:10.1073/pnas.2103196118
- Lee, A., Scapa, E., Cohen, D., and Glimcher, L. (2008). Regulation of hepatic lipogenesis by the transcription factor XBP1. *Science* 320 (5882), 1492–1496. doi:10.1126/science.1158042
- Lee, E. J., Chiang, W. C. J., Kroeger, H., Bi, C. X., Chao, D. L., Skowronska-Krawczyk, D., et al. (2020). Multiexon deletion alleles of ATF6 linked to achromatopsia. *JCI Insight* 5 (7), e136041. doi:10.1172/jci.insight.136041
- Martino, F., Chen, X., Lee, A.-H., and Glimcher, L. H. (2010). TLR activation of the transcription factor XBP1 regulates innate immune responses in macrophages. *Nat. Immunol.* 11 (5), 411–418. doi:10.1038/ni.1857
- Mendes, A., Gigan, J. P., Rodrigues, C. R., Choteau, S. A., Sanseau, D., Barros, D., et al. (2020). Proteostasis in dendritic cells is controlled by the PERK signaling axis independently of ATF4. *Life Sci. Alliance* 4 (2), 2020008655–e202000922. doi:10.26508/lsa.202000865
- Mogilenko, D. A., Haas, J. T., L'homme, L., Fleury, S., Quemener, S., Levasseur, M., et al. (2019). Metabolic and innate immune cues merge into a specific inflammatory response via the UPR. *Cell* 177 (5), 1201–1216. doi:10.1016/j.cell.2019.03.018
- Murphy, T. L., Grajales-Reyes, G. E., Wu, X., Tussiwand, R., Briseño, C. G., Iwata, A., et al. (2016). Transcriptional control of dendritic cell development. *Annu. Rev. Immunol.* 34 (1), 93–119. doi:10.1146/annurev-immunol-032713-120204
- Osorio, F., Tavernier, S. J., Hoffmann, E., Saeys, Y., Martens, L., Veters, J., et al. (2014). The unfolded-protein-response sensor IRE-1α regulates the function of CD8α⁺ dendritic cells. *Nat. Immunol.* 15 (3), 248–257. doi:10.1038/ni.2808
- Read, A., and Schröder, M. (2021). The unfolded protein response: An overview. *Biol. (Basel)* 10 (5), 384–410. doi:10.3390/biology10050384
- Sharma, R. B., Snyder, J. T., and Alonso, L. C. (2019). Atf6a impacts cell number by influencing survival, death and proliferation. *Mol. Metab.* 27, S69–S80. doi:10.1016/j.molmet.2019.06.005
- Shoulders, M. D., Ryno, L. M., Genereux, J. C., Moresco, J. J., Tu, P. G., Wu, C., et al. (2013). Stress-independent activation of XBPs and/or ATF6 reveals three functionally diverse ER proteostasis environments. *Cell Rep.* 3 (4), 1279–1292. doi:10.1016/j.celrep.2013.03.024
- Smith, H. L., Freeman, O. J., Butcher, A. J., Holmqvist, S., Humoud, I., Schätzl, T., et al. (2020). Astrocyte unfolded protein response induces a specific reactivity state that causes non-cell-autonomous neuronal degeneration. *Neuron* 105 (5), 855–866. doi:10.1016/j.neuron.2019.12.014
- Sun, T., Nguyen, A., and Gommerman, J. L. (2020). Dendritic cell subsets in intestinal immunity and inflammation. *J. Immunol.* 204 (5), 1075–1083. doi:10.4049/jimmunol.1900710

Publisher's note

All claims expressed in this article are solely those of the authors and do not necessarily represent those of their affiliated organizations, or those of the publisher, the editors and the reviewers. Any product that may be evaluated in this article, or claim that may be made by its manufacturer, is not guaranteed or endorsed by the publisher.

Supplementary material

The Supplementary Material for this article can be found online at: <https://www.frontiersin.org/articles/10.3389/fcell.2023.1089728/full#supplementary-material>

Tavernier, S. J., Osorio, F., Vandersarren, L., Veters, J., Vanlangenakker, N., Van Isterdael, G., et al. (2017). Regulated IRE1-dependent mRNA decay sets the threshold for dendritic cell survival. *Nat. Cell Biol.* 19 (6), 698–710. doi:10.1038/ncb3518

Therauf, D. J., Marcinko, M., Belmont, P. J., and Glembotski, C. C. (2007). Effects of the isoform-specific characteristics of ATF6 α and ATF6 β on endoplasmic reticulum stress response gene expression and cell viability. *J. Biol. Chem.* 282 (31), 22865–22878. doi:10.1074/jbc.M701213200

Therauf, D. J., Morrison, L., and Glembotski, C. C. (2004). Opposing roles for ATF6 α and ATF6 β in endoplasmic reticulum stress response gene induction. *J. Biol. Chem.* 279 (20), 21078–21084. doi:10.1074/jbc.M400713200

Therauf, D. J., Morrison, L. E., Hoover, H., and Glembotski, C. C. (2002). Coordination of ATF6-mediated transcription and ATF6 degradation by a domain that is shared with the viral transcription factor, VP16. *J. Biol. Chem.* 277 (23), 20734–20739. doi:10.1074/jbc.M201749200

Vidal, R. L., Sepulveda, D., Troncoso-Escudero, P., Garcia-Huerta, P., Gonzalez, C., Plate, L., et al. (2021). Enforced dimerization between XBP1s and ATF6f enhances the protective effects of the UPR in models of neurodegeneration. *Mol. Ther.* 29 (5), 1862–1882. doi:10.1016/j.ymthe.2021.01.033

Yamamoto, K., Sato, T., Matsui, T., Sato, M., Okada, T., Yoshida, H., et al. (2007). Transcriptional induction of mammalian ER quality control proteins is mediated by

single or combined action of ATF6 α and XBP1. *Dev. Cell* 13 (3), 365–376. doi:10.1016/j.devcel.2007.07.018

Yamamoto, K., Yoshida, H., Kokame, K., Kaufman, R. J., and Mori, K. (2004). Differential contributions of ATF6 and XBP1 to the activation of endoplasmic reticulum stress-responsive cis-acting elements ERSE, UPRE and ERSE-II. *J. Biochem.* 136 (3), 343–350. doi:10.1093/jb/mvh122

Yoshida, H., Haze, K., Yanagi, H., Yura, T., and Mori, K. (1998). Identification of the cis-acting endoplasmic reticulum stress response element responsible for transcriptional induction of mammalian glucose-regulated proteins: Involvement of basic leucine zipper transcription factors. *J. Biol. Chem.* 273 (50), 33741–33749. doi:10.1074/jbc.273.50.33741

Yoshida, H., Matsui, T., Yamamoto, A., Okada, T., and Mori, K. (2001). XBP1 mRNA is induced by ATF6 and spliced by IRE1 in response to ER stress to produce a highly active transcription factor. *Cell* 107, 881–891. doi:10.1016/s0092-8674(01)00611-0

Yoshida, H., Okada, T., Haze, K., Yanagi, H., Yura, T., Negishi, M., et al. (2000). ATF6 activated by proteolysis binds in the presence of NF-Y (CBF) directly to the cis-acting element responsible for the mammalian unfolded protein response. *Mol. Cell Biol.* 20 (18), 6755–6767. doi:10.1128/mcb.20.18.6755-6767.2000